ADVANCING EARTH AND SPACE SCIENCE

JGR Oceans

RESEARCH ARTICLE
10.1029/2022JC019470

Adam V. Subhas and Frank J. Pavia contributed equally to this work.

Key Points:

- Particle data from large-volume pumps was compiled globally
- Particles collected with pumps are enriched in organic carbon compared with sediment traps
- Rapidly sinking particles appear efficient at delivering minerals to the deep ocean and the seafloor

Supporting Information:

Supporting Information may be found in the online version of this article.

Correspondence to:

A. V. Subhas, F. J. Pavia and S. Dong,
asubhas@whoi.edu;
fjpavia@caltech.edu;
dongsijia.nju@gmail.com

Citation:

Subhas, A. V., Pavia, F. J., Dong, S., & Lam, P. J. (2023). Global trends in the distribution of biogenic minerals in the Ocean. *Journal of Geophysical Research: Oceans*, *128*, e2022JC019470. https://doi.org/10.1029/2022JC019470

Received 8 NOV 2022
Accepted 27 JAN 2023

Author Contributions:

Conceptualization: Adam V. Subhas, Frank J. Pavia, Sijia Dong
Data curation: Frank J. Pavia, Sijia Dong, Phoebe J. Lam
Formal analysis: Adam V. Subhas, Frank J. Pavia, Phoebe J. Lam
Project Administration: Adam V. Subhas
Visualization: Frank J. Pavia
Writing – original draft: Adam V. Subhas
Writing – review & editing: Adam V. Subhas, Frank J. Pavia, Sijia Dong, Phoebe J. Lam

Global Trends in the Distribution of Biogenic Minerals in the Ocean

Adam V. Subhas[1], Frank J. Pavia[2], Sijia Dong[3], and Phoebe J. Lam[4]

[1]Department of Marine Chemistry and Geochemistry, Woods Hole Oceanographic Institution, Falmouth, MA, USA, [2]Division of Geological and Planetary Sciences, California Institute of Technology, Pasadena, CA, USA, [3]School of Geography and Ocean Science, Nanjing University, Nanjing, China, [4]Department of Ocean Sciences, University of California Santa Cruz, Santa Cruz, CA, USA

Abstract The cycling of marine particulate matter is critical for sequestering carbon in the deep ocean and in marine sediments. Biogenic minerals such as calcium carbonate ($CaCO_3$) and opal add density to more buoyant organic material, facilitating particle sinking and export. Here, we compile and analyze a global data set of particulate organic carbon (POC), particulate inorganic carbon (PIC, or $CaCO_3$), and biogenic silica (bSi, or opal) concentrations collected using large volume pumps (LVPs). We analyze the distribution of all three biogenic phases in the small (1–53 μm) and large (>53 μm) size classes. Over the entire water column 76% of POC exists in the small size fraction. Similarly, the small size class contains 82% of PIC, indicating the importance of small-sized coccolithophores to the PIC budget of the ocean. In contrast, 50% of bSi exists in the large size fraction, reflecting the larger size of diatoms and radiolarians compared with coccolithophores. We use PIC:POC and bSi:POC ratios in the upper ocean to document a consistent signal of shallow mineral dissolution, likely linked to biologically mediated processes. Sediment trap PIC:POC and bSi:POC are elevated with respect to LVP samples and increase strongly with depth, indicating the concentration of mineral phases and/or a deficit of POC in large sinking particles. We suggest that future sampling campaigns pair LVPs with sediment traps to capture the full particulate field, especially the large aggregates that contribute to mineral-rich deep ocean fluxes, and may be missed by LVPs.

Plain Language Summary In the surface ocean, organisms produce minerals along with the organic carbon that fuels most marine life. A portion of this material sinks to the deep ocean, which is driven by the formation of large aggregates and the ballasting effect of dense biominerals. Here we investigate a global compilation of particulate material in the ocean and compare it to a recent compilation of sinking material collected by sediment traps. We find that large, sedimenting particles contain much less organic carbon relative to the amount of biominerals, compared to smaller particles collected on filters. This result has implications for both the processing of organic carbon and biominerals in the ocean, and the delivery of minerals and organic carbon to the deep ocean and to the seafloor.

1. Introduction

Dissolved inorganic carbon in the surface ocean is fixed into organic matter by phytoplankton through photosynthesis, creating the biomass that fuels the marine food web and driving air-sea exchange of carbon dioxide (CO_2). A portion of this biologically produced particulate matter sinks into the deep ocean, a process known as the biological carbon pump (BCP, Volk & Hoffert, 1985). Most particulate organic carbon (POC) is only slightly denser than seawater (Alldredge & Gotschalk, 1988) and does not sink readily on its own. Therefore, processes that create particles dense enough to sink out of the surface ocean are critical for the BCP to function, either through the association of POC with dense mineral phases (Klaas & Archer, 2002), or through the formation of larger particle aggregates (McCave, 1975). The size, mineral content, and porosity of biological material all influence the efficiency of vertical POC transport, and these characteristics are directly related to the biological communities that produce and consume this material.

Because they are significantly denser than seawater, the biologically produced minerals biogenic silica (bSi) and calcium carbonate ($CaCO_3$, also known as particulate inorganic carbon or PIC) provide ballast for the BCP. In addition to its ballasting role, PIC formation decreases alkalinity and raises seawater pCO_2 (Frankingouille et al., 1994; Humphreys et al., 2018). The counteracting effects of CO_2 drawdown by enhancing ballast, and

CO_2 release by alkalinity consumption, means that the PIC:POC export ratio influences the partitioning of CO_2 between the atmosphere and the ocean (Sarmiento et al., 2002). The formation of biogenic silica (bSi), on the other hand, provides ballast without any direct impact on the seawater dissolved carbonate system. The relative export of bSi and POC (bSi:POC) therefore exerts its own influence on the transfer efficiency of particulate carbon and the sequestration of CO_2 in the deep ocean. Thus, the partitioning of carbon throughout the water column is influenced not only by the export of POC, but also by PIC:POC and bSi:POC ratios.

The relationships between POC, mineral ballasting, and the sequestration of carbon in the deep ocean remain poorly constrained (Fowler & Knauer, 1986; Laurenceau-Cornec et al., 2020). It has long been recognized that particle size may influence sinking rates to a greater extent than mineral content (McCave, 1984). Many organisms that produce dense biominerals are also small, meaning that their sinking rates will be dictated by the same aggregation/disaggregation processes that control particle size regardless of mineral content. While bSi and PIC are hypothesized to be more resistant to remineralization than POC, there is substantial and growing evidence that a large portion of these mineral phases dissolve in the upper water column, predominantly through biologically mediated pathways (Bidle & Azam, 1999; Feely et al., 2002; Milliman et al., 1999; Subhas et al., 2022; Sulpis et al., 2021). These processes may decrease the influence of mineral ballasting on carbon export. The size distribution of these mineral phases; their susceptibility to dissolution during export; and thus their overall influence on the BCP; are all still open questions (Passow & De La Rocha, 2006; Xiang et al., 2022).

The traditional method for quantifying sinking fluxes of organic carbon and biogenic minerals is through collection and analysis of actively sinking particles in containers called sediment traps (STs, Martin et al., 1987). In contrast to STs that directly measure particle fluxes, the growing use of large-volume pumps (LVPs) has provided an alternative approach to collect and analyze particle concentrations (Bishop et al., 1980; Lam et al., 2018). LVPs collect the particulate material at a given depth in the water column by pumping 100–1,000s of liters of water through filters. Many LVP deployments use paired filters of different mesh sizes in series, collecting particle samples in distinct size classes. The size-fractionated particle concentration, and the composition of these particles, has been translated into sinking velocity and mass flux using empirical (or semi-empirical) relationships between particle size and sinking velocity (Bishop et al., 1977; Guidi et al., 2008; Laurenceau-Cornec et al., 2020; Xiang et al., 2022).

Theoretically, both sediment traps and large-volume pumps should capture a wide size range of marine particles that are associated with a spectrum of sinking velocities and mass fluxes (Cael et al., 2021; Guidi et al., 2008). However, it is critical to assess whether measurements of particle concentration from LVPs show the same distributions of organic carbon and ballasting minerals as measurements of particle flux from STs. If sediment traps and LVPs exhibit unique distributions of PIC, POC, and bSi, then the derived particle fluxes from LVPs may not be directly comparable to ST fluxes. In this work, we compare a newly compiled LVP particulate data set (Pavia et al., 2022) with a recent compilation of global ST particle fluxes (Mouw et al., 2016). We use the resulting trends to speculate on the drivers of POC, PIC, and bSi cycling in the ocean, and the fate of these phases in the water column and in sediments.

2. Materials and Methods

2.1. Data Sets

We merged the Multiple Unit Large Volume in situ Filtration System (MULVFS, Bishop et al., 1985) LVP PIC, POC, and bSi data set, published partially in Lam et al. (2011) and references therein, with data collected using McLane in situ pumps equipped with two size-fractionating filters during the GA03 (Lam et al., 2015) and GP16 (Lam et al., 2018) cruises of the U.S. GEOTRACES program. All data are available from BCO-DMO (Bishop & Lam, 2022; Pavia et al., 2022). The filter sizes generally consist of a 51 or 53 μm pre-filter that collects large particles, followed by a 0.8 or 1 μm filter that collects smaller particles. We annotate large size fraction particles (>53 or >51 μm) as "LSF," and small size fraction particles (1–53 or 0.8–51 μm) denoted "SSF" (small size fraction).

The Mouw et al. (2016) data set contains quality-controlled fluxes of POC, PIC, and bSi across different types of sediment traps at depths distributed throughout the water column. For bottom-moored sediment traps deployed for many months at a time, this data set contains fluxes from individual cups (~15–30 days intervals), rather than the average fluxes across the entire annual duration of the ST deployment. Another ST compilation from Honjo et al. (2008) presents annually averaged data, which may be suitable for the deep ocean but could lead to

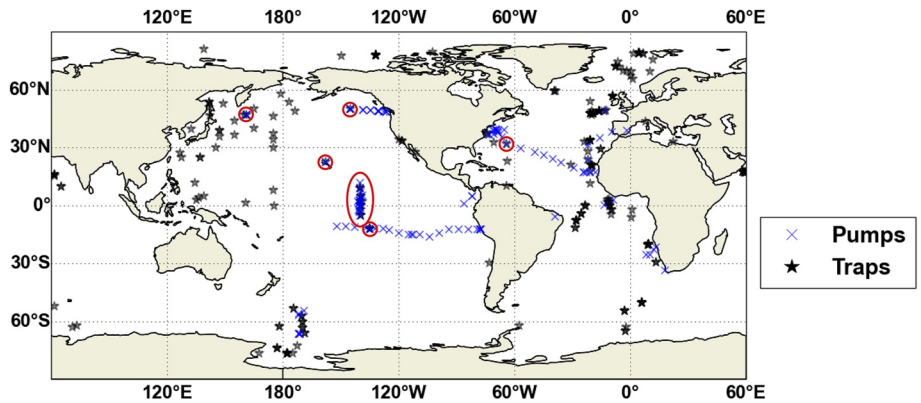

Figure 1. Locations of large-volume pump data compiled for this paper (blue x's), and previously compiled trap data (black stars, Mouw et al., 2016). We show cotemporal pump-trap comparisons at the locations circled in red in Section 3.

sampling biases in the shallow ocean. Individual cup analyses may provide a closer comparison to LVP data that are collected over short (Figure 4h) deployments, and therefore we compare our LVP compilation to the Mouw et al. (2016) data set.

The LVP and ST data sets both demonstrate sample coverage across the world oceans (Figure 1). While the ST data set has more data from the North Pacific and Eastern Atlantic, the pump data set has more samples from the subtropics in the South Pacific and North Atlantic. For initial comparisons, data sets were matched both in space and in time. Locations with ST timeseries such as Station ALOHA and Ocean Station PAPA (OSP) could be compared with LVP data collected to within 1 month of each other. In other locations such as K2, both LVPs and sediment traps were deployed concurrently, allowing for contemporaneous comparisons of the two methods (Bishop & Wood, 2008; Lamborg et al., 2008).

2.2. Sample Analysis and Quality Control

The GEOTRACES datasets were quality controlled upon being merged with the MULVFS data set. Data marked as "questionable" or "bad," such as from known sampling or analytical issues, were excluded. In total, this compilation includes 987 paired LSF-SSF data points. All data are quality-controlled and the compilation is available online (see Data Availability Statement). Data were generally acquired using an elemental analyzer for POC concentrations, coulometry or Ca^{2+} analysis for PIC concentrations, and spectrophotometry for bSi concentrations, and are blank-corrected using analysis of dipped blank filters (e.g., Lam et al., 2018). In the MULVFS data set, we exclude data from artificial iron fertilization experiments in the Southern Ocean because the point of these experiments was to purposely alter natural carbon export fluxes from the surface ocean. Statistical analyses discussed in this paper use all the quality-controlled data in our data set, and the quality-controlled ST data presented in Mouw et al. (2016).

3. Results

3.1. Concentration Profiles

We compiled global profiles of LSF and SSF PIC, POC, and bSi (Figure 2). For POC, both the LSF and SSF exhibit the highest concentrations at the surface (~1–10 μmol L^{-1}, Figure 2a). Concentrations decrease rapidly with depth in the upper 500–1,000 m, and demonstrate relatively constant values in the deeper water column. We note a slight increase in POC and bSi concentration below 4,500 m. Over the entire water column, the SSF POC concentration is higher than the LSF concentration. In general, POC exhibits more variability in the upper water column than deeper. The LSF demonstrates larger variability than the SSF throughout the entire water column, but this is especially the case in the upper 1,000 m (Figure 2a).

The SSF PIC demonstrates a large concentration range near the surface, and values converge with depth over the upper 500 m (Figure 2b). The apparent increase in minimum PIC with depth that we observe in this global compilation is also evident in multiple Pacific Ocean sections (Dong et al., 2019; Lam & Marchal, 2015; Lam et al., 2018). Similar to POC, SSF, PIC is also higher than LSF throughout the water column (Figure 2b). Variability in PIC

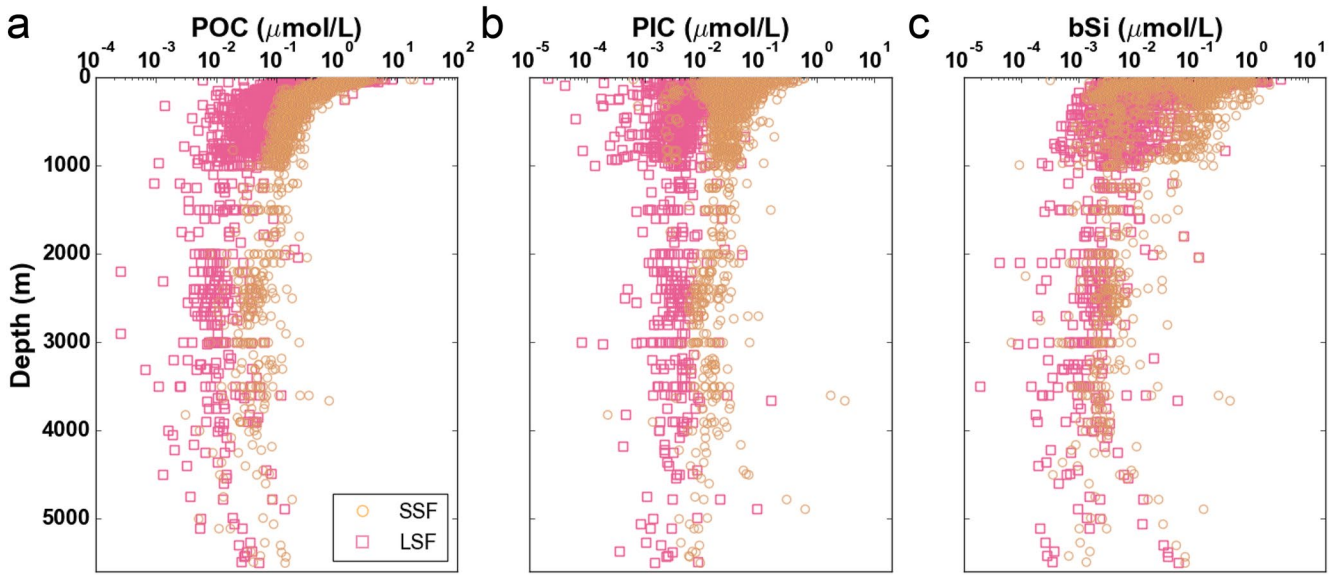

Figure 2. Globally compiled large-volume pump concentration profiles of (a) particulate organic carbon, (b) particulate inorganic carbon, and (c) biogenic silica in the small size fraction (yellow circles) and large size fraction (pink squares). Concentrations are plotted on a log-scale.

concentration decreases with depth. The bSi profiles demonstrate distinct profile shapes compared with POC and PIC (Figure 2c). Especially in the SSF, there are two distinct groupings in the upper 1,000 m, one at higher bSi, and one at lower bSi. These two profile groups appear to be related to geographic differences in bSi concentration, with high-bSi data originating from coastal and high-productivity areas, and low-bSi data coming from oligotrophic regions (Figure S1 in Supporting Information S1). In contrast to both POC and PIC, the differences between SSF and LSF bSi concentrations are smaller (Figure 2c). We observe several high bSi points between 4,000 and 5,000 m, initiating around the same depth as the observed increase in POC (Figures 2a and 2c). These points originate from the GA03 and GP16 GEOTRACES legs, and are likely influenced by coastal/downslope transport and/or the intense primary production in the Peru upwelling region (Lam et al., 2018).

3.2. Ratios of Mineral Content to POC

Ratios of mineral content to POC in pump and ST samples can be used to infer biological or chemical processes in the water column (Dong et al., 2022). From the concentration and ST flux profiles, we calculate molar ratios of PIC and bSi to POC (PIC:POC and bSi:POC, respectively) in the SSF, LSF, and ST pools. Because of the sampling location differences between pump and trap data sets (Figure 1), it is possible that geographic and temporal differences may bias any direct comparisons of these two sampling methods. We attempt to minimize temporal and spatial sampling biases by directly comparing SSF, LSF, and ST data at stations where all measurements occurred within 1 month of each other for both PIC:POC (Figure 3) and bSi:POC (Figure 4). These stations include multiple locations in the Equatorial Pacific (Figures 3 and 4a–4g), Station ALOHA (Figure 4h), three time periods at Ocean Station Papa (OSP, Figures 4i–4k), two time periods at Station K2 in the western Subarctic Pacific (Figures 4l and 4m), and one time interval at the Bermuda Atlantic Timeseries (BATS, Figure 4n). For stations with data spanning multiple months or years, we highlight the cotemporal ST data with bold markers, and show asynchronous data as transparent symbols in the background (e.g., Figure 3i).

We acknowledge that our analyses originate from a range of trap types and oceanographic conditions. We suggest that comparing the different trap types compiled by Mouw et al. (2016) does not introduce a major bias in PIC:POC and bSi:POC. For example, fluxes measured using neutrally buoyant sediment traps and standard particle interceptor traps show only minor offsets from each other (Baker et al., 2020; Buesseler et al., 2008; Lamborg et al., 2008). In addition, the upper ocean OSP data originates from a moored trap at 200 m and a free-drifting trap array, with little indication of offsets in the structure of PIC:POC and bSi:POC (Figures 3 and 4i–4k). The influence of current speed is also likely minimal, as exemplified by the consistent offsets between ST and LVP data at OSP despite highly variable current speeds from March through August at this location (National Data Buoy Center Station 46246).

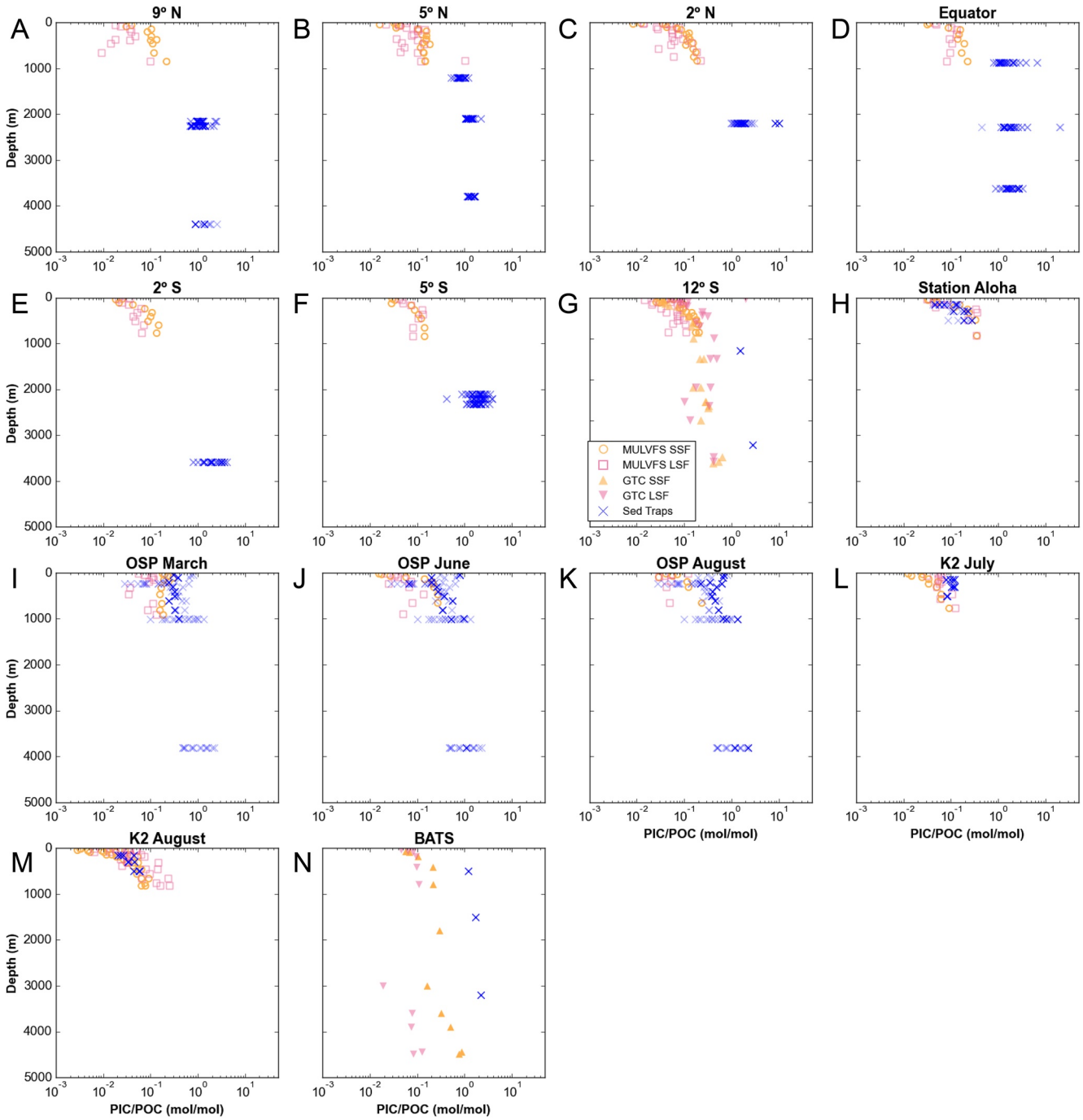

Figure 3. Co-located and cotemporal measurements of particulate inorganic carbon:particulate organic carbon at multiple locations. Sediment trap (ST) data that are temporally matched to pump data are shown as solid blue X's; transparent markers are ST data from the same location but not the same time period. Multiple Unit Large Volume in-situ Filtration System and ST data in panels (a–g) from JGOFS Equatorial Pacific cruises along 135°W in 1992 (Honjo et al., 1995; Lam et al., 2011); in panels (i–k) from Canadian JGOFS cruises in 1996–1997 (Lam et al., 2011; Timothy et al., 2013; Wong et al., 1999); in panels (h, l, and m) from VERTIGO cruises in 2004–2005 (Bishop & Wood, 2008; Lamborg et al., 2008). Geotraces data in panel (g) from GP16 GEOTRACES cruise at 12°S, 133°W and 12°S, 137°W in 2013 (Lam et al., 2018); in panel (n) from GA03 GEOTRACES cruise in 2011 (Lam et al., 2015). ST data in panel (n) from the Ocean Flux Program (Conte, 2022).

At all times and stations, SSF and LSF exhibit similar PIC:POC (Figure 3). At 12°S, we observe a good correspondence between Geotraces (GT) and MULVFS SSF PIC:POC data despite sampling dates over 20 years apart (Figure 3g). A greater difference is observed between the LSF PIC:POC from these two campaigns, which may be explained by a greater temporal variability in large PIC producers, either seasonally or interannually (Figure 3g).

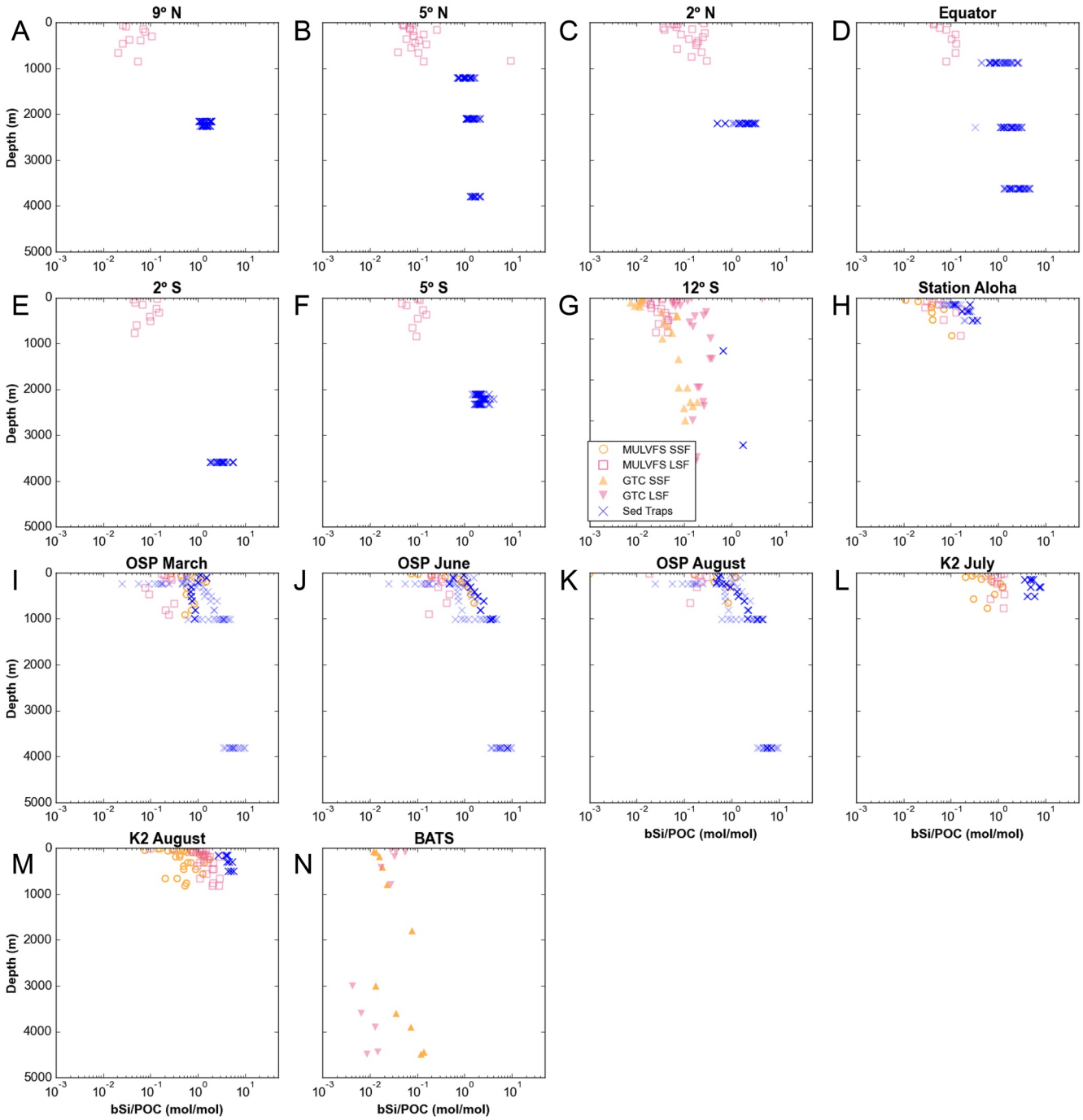

Figure 4. Co-located and cotemporal measurements of biogenic silica:particulate organic carbon at multiple locations. See Figure 3 caption for sampling details.

Nevertheless, ST data from the MULVFS era exhibit higher PIC:POC than either of the LVP pump sampling campaigns. Indeed, across all locations, ST PIC:POC are often higher than SSF and LSF values from LVP. Notable exceptions to this trend are found at Station ALOHA (Figure 3h) and at K2 in August (Figure 3m), where ST PIC:POC falls directly on top of the SSF and LSF. Sediment trap PIC:POC is therefore always either the same or higher than SSF and LSF PIC:POC at all times and locations investigated here.

We observe similar patterns in bSi:POC at these times and locations (Figure 4). Although SSF data are not available for much of the equatorial Pacific, sediment traps appear consistently enriched in bSi relative to the LSF (Figures 4a–4g). In stations where SSF bSi are available, the LSF is often enriched in bSi relative to the

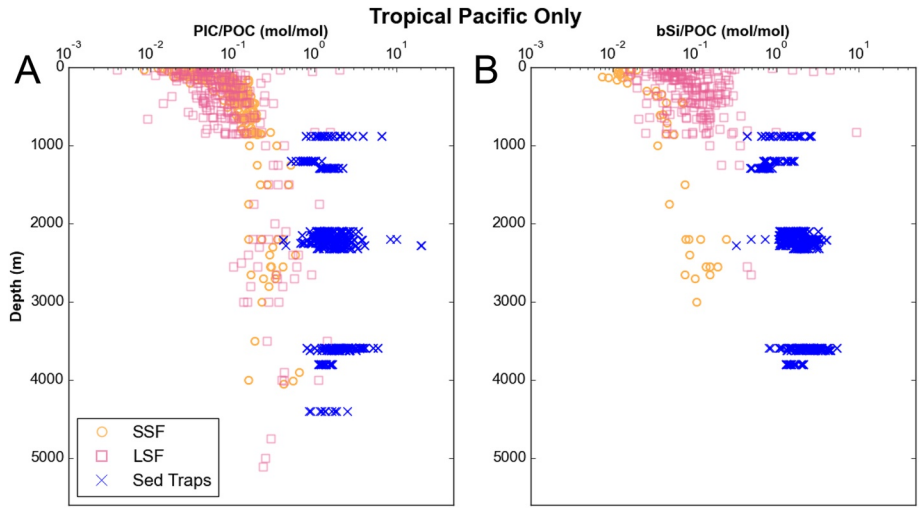

Figure 5. Comparison of (a) particulate inorganic carbon:particulate organic carbon (POC) and (b) biogenic silica:POC across all particle types in the tropical Pacific (12°S–9°N along 135°W). These geographically restricted data show similar trends to the global compilation.

SSF (Figures 4g, 4h, and 4l–4n), since diatoms are often produced directly into the LSF. At OSP, where large diatom growth may be iron-limited, bSi:POC is greater in the SSF compared to LSF (Figures 4i–4k). As with PIC:POC, the GT LSF bSi:POC sampled in 2013 appears enriched relative to the MULVFS data sampled in 1992 (Figure 4g). Sediment trap bSi:POC is enriched relative to the SSF and the LSF in most locations, with the exception of OSP where it appears to closely track the SSF bSi:POC (Figures 4i–4k). Unlike the PIC:POC distributions, the sediment traps at Station ALOHA and K2 in August exhibit enrichment in bSi:POC relative to the SSF and LSF (Figure 4h). In summary, as with PIC:POC, sediment traps generally exhibit either similar or elevated bSi:POC relative to SSF and LSF samples.

The equatorial Pacific stations and Station ALOHA demonstrate relatively low variability in ST flux composition (Figures 3 and 4a–4h), as evidenced by the overlap between the solid and transparent points at these locations. Compared to the equator and the subtropics, OSP exhibits more ST variability (Figures 3 and 4i–4k). The low temporal variability in tropical Pacific ST data, combined with the depth coverage for both sediment traps and LVPS at these locations, allows us to ask whether this region exhibits consistent trends in PIC:POC and bSi:POC across all time periods. We compiled all available data from the Tropical Pacific (12°S–9°N), and observe similar trends to the individual locations, with PIC:POC SSF and LSF data falling mostly on top of each other and sediment traps being elevated relative to both filtered fractions (Figure 5a). The bSi:POC data show a similar ST enrichment relative to both filtered fractions (Figure 5b). In addition, the LSF appears to be enriched relative to the SSF at all depths.

Following on the consistency of the Tropical Pacific relationship regardless of temporal matching, we now ask whether these same trends appear in global PIC:POC and bSi:POC compilations across all time intervals and locations. This global analysis is further justified by the trends observed at OSP (Figures 3 and 4i–4k). These stations indicate that ST PIC:POC and bSi:POC consistently fall either equal to or higher than the LVP data when matched in time. The temporal variability in ST data creates greater overlap with the LVP data; therefore comparing all data regardless of time provides a lower bound on the separation between ST and LVP mineral:POC ratios.

Global profiles of PIC:POC are presented as depth-binned box plots for the SSF (Figure 6a), LSF (Figure 6b), and ST datasets (Figure 6c, Mouw et al., 2016). In each data set, PIC:POC increases with depth, especially in the upper ~1,500 m, consistent with the short remineralization length scale of POC relative to mineral phases (Dunne et al., 2007). Surface ratios in all data sets demonstrate the highest variability, and this variability decreases with depth. The surface median SSF PIC:POC value of ~0.04 increases with depth to a maximum value of ~0.25 between 3,500 and 4,500 m (Figure 6a). Similarly, the median LSF PIC:POC of ~0.05 increases to a value of ~0.5 at 2,750 m, before decreasing again to a value of ~0.3 in the deepest water column (Figure 6b). In contrast to the filtered fractions, surface sediment traps demonstrate a much higher median PIC:POC (0.4, Figure 6c), and these values also increase with depth to >1 in the deep ocean.

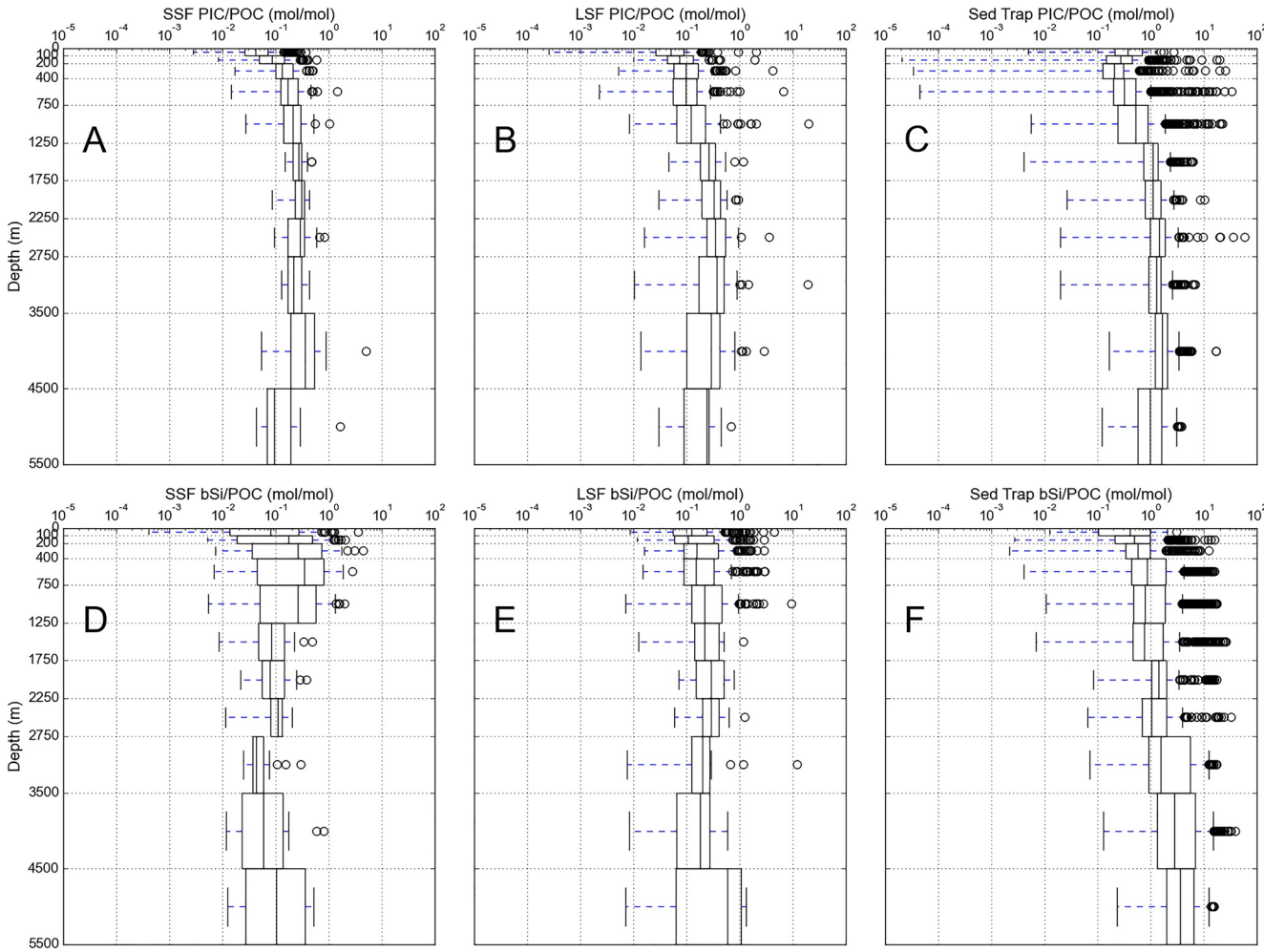

Figure 6. Particulate inorganic carbon:particulate organic carbon (POC), plotted as box-and-whisker distributions in depth bins, for (a) small size fraction large volume pump (LVP) data, (b) large size fraction LVP data, and (c) sediment trap data. (d–f) Are the same as (a–c) except for biogenic silica:POC. The line denotes the median value for each depth bin. The box denotes the first quartile of all data for each depth bin. The whiskers denote the third quartile for each depth bin. Individual outliers are displayed as circles.

As with PIC:POC, bSi:POC ratios increase slightly with depth, although there is substantial variability throughout the water column (Figures 6d–6f). The median surface SSF bSi:POC is about 0.07, which increases to a maximum value of 0.3 between 400 and 750 m, before decreasing again to ~0.1 through the deeper water column (Figure 6d). This mesopelagic maximum in SSF bSi:POC appears to be related to higher SSF bSi concentrations sampled by MULVFS above ~1,000 m (Figure 2c). MULVFS deployments only sampled in the upper 1,000 m, whereas McLane pumps deployed on the GEOTRACES expeditions sampled the entire water column. Further, MULVFS sampled in high diatom regions such as the Antarctic and Western Subarctic Pacific, whereas GEOTRACES samples were concentrated in subtropical gyres (Figure S1 in Supporting Information S1). The mesopelagic maximum in SSF bSi:POC is thus likely due to the influence of MULVFS samples from high diatom regions. The median surface LSF bSi:POC is slightly elevated relative to the SSF, and does not show the same mesopelagic maximum (Figure 6e). The bifurcation of bSi concentration in the deep ocean (Figure 2c) manifests as a large variability in bSi:POC in the SSF and LSF data sets (Figures 6d and 6e). The median surface ST bSi:POC (0.4, Figure 6f) is enriched relative to both the SSF and LSF, and indicates that sinking ST material is enriched in silica relative to the majority of the particulate pool captured by LVPs. This enrichment continues into the deep ocean, where the median ST bSi:POC at 4,500 m (3.5) is over an order of magnitude greater than the median SSF and LSF deep ocean values. Such enrichment has been observed in other select locations (Figures 4 and 5, Buesseler et al., 2001; Honjo et al., 2008), and through this analysis it appears to be a global feature of ST material.

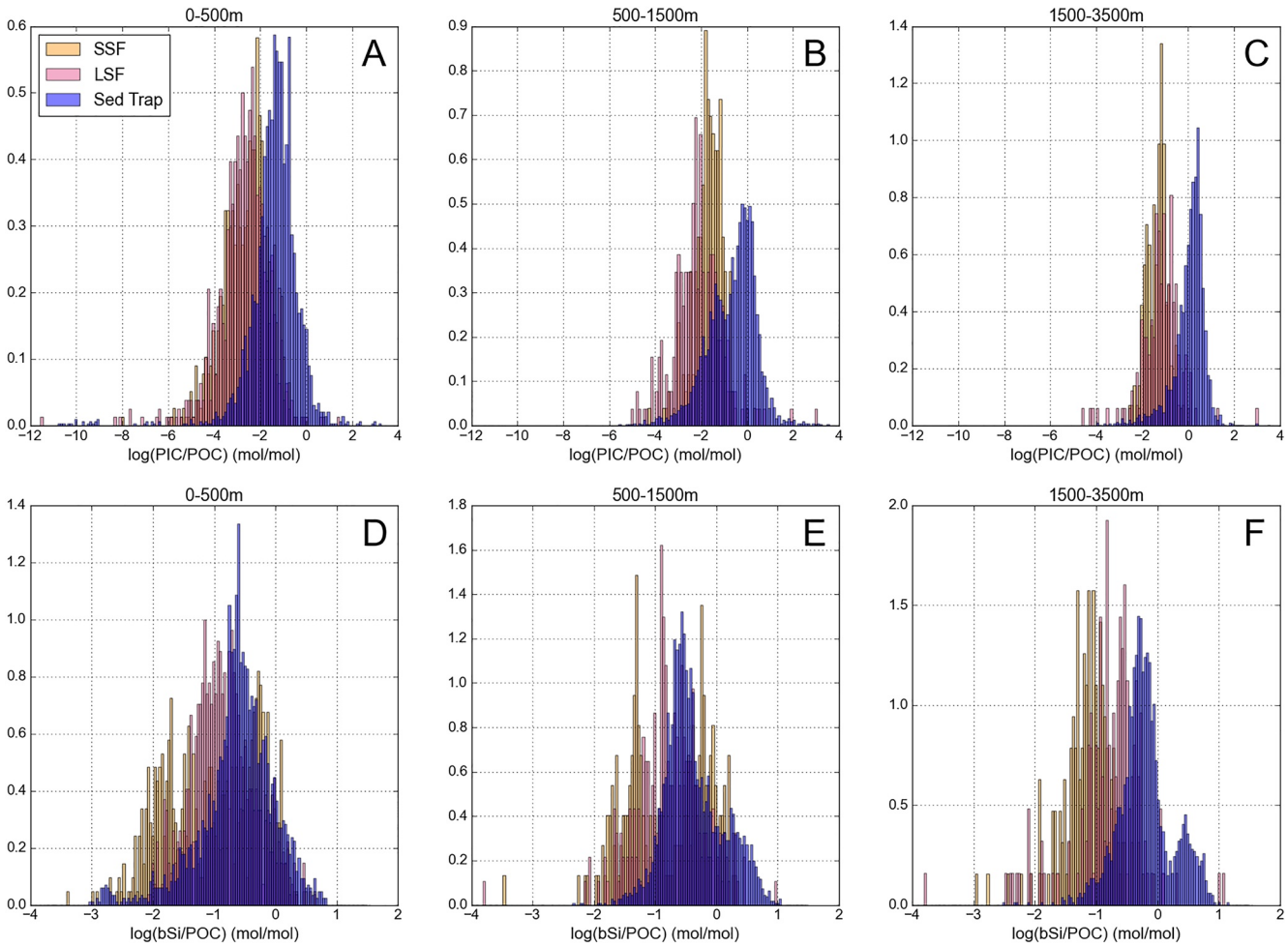

Figure 7. Distributions of (a–c) Particulate inorganic carbon:particulate organic carbon (POC) and (d–f) biogenic silica:POC in small size fraction (yellow), large size fraction (pink), and Sediment trap (blue) samples. Ratios are in log10 scale. Each plot is for a specific depth bin: (a, d) 0–500 m, (b, e) 500–1,500 m, and (c, f) 1,500–3,500 m.

The box plot distributions of PIC:POC and bSi:POC (Figure 6) suggest distributions with long, low mineral:POC tails, and sharp, high mineral:POC boundaries with only a few outliers on the high ratio side. This feature is common to all size classes and all depth bins. We compiled histograms of PIC:POC and bSi:POC, overlaying the SSF, LSF, and ST distributions for three representative depth bins: 0–500, 500–1,500, and 1,500 m-bottom (Figure 7). While these histograms are illustrative, they do not represent true probability distribution functions, because they are plotted on a logarithmic *x*-axis—therefore bin widths appear equal on a logarithmic scale, but are not actually equal width. The *y*-axes of these distributions denote the relative proportion of values within each value bin. Absolute *y*-values can be compared within each panel, but not between panels.

For PIC:POC, there is significant overlap between the LSF and SSF distributions at all depths (Figures 7a–7c). Sediment trap PIC:POC either overlaps with, or is enriched relative to, the filtered fractions, consistent with our regional observations of PIC:POC (Figure 3). We note that this comparison is done with all data without temporal matching. For instance, using exclusively temporally matched data at OSP would create larger offsets between STs and LVPs (Figures 3i–3k). While more LVP data would certainly improve our interpretations, these offsets appear to be a robust feature of the global data set, after considering both temporal and regional differences (Figures 3–5).

The separation between ST and LVP data grows with depth. We observe two distinct peaks in ST PIC:POC in the mesopelagic: One directly overlapping with the filtered SSF and LSF fractions, and one larger peak with distinctly higher PIC:POC (Figure 7b). This bimodal distribution may reflect spatial and temporal differences

in production ecology and food web structure (Section 4.1). Aside from differences in the filtered fractions, the STs consistently demonstrate the highest PIC:POC ratios at all depths, with a distribution that only marginally overlaps with LVPs below 1,500 m (Figure 7c). The median ST PIC:POC in the deep ocean is enriched by almost two orders of magnitude relative to both SSF and LSF particles, and demonstrates a long, low-PIC:POC tail with a sharp, high-PIC:POC cutoff around a value of about 10 mol PIC/mol POC.

Unlike PIC:POC, the 0–500 m SSF demonstrates a bimodal bSi:POC distribution (Figure 7d), related to the two distinct bSi profile shapes in the upper 1,000 m (Figure 2c). The LSF demonstrates a single peak in the middle of the SSF distribution. Part of the SSF distribution is about an order of magnitude depleted in bSi relative to the LSF (Figure 7d). Although there is some overlap, sediment traps consistently fall at the upper end of the LVP size fraction distributions. In the mesopelagic between 500 and 1,500 m, the ST distribution develops a high bSi:POC shoulder that is distinct from SSF and LSF distributions, reaching values of up to 10 mol/mol (Figure 7e). Deeper in the water column, the ST distribution diverges toward higher bSi:POC and the high-ratio peak becomes even more distinct from filtered data (Figure 7f). This secondary peak appears to be geographically distinct, with most of the very high bSi:POC ratios coming from the Western Subarctic North Pacific and the Southern Ocean (Figure S2 in Supporting Information S1), two regions that are known to have very high diatom production and export (Buesesler et al., 2001; Honjo et al., 2008; Hou et al., 2019). These regions coincide with high bSi concentrations as well (Figure S1 in Supporting Information S1), tying the distribution of bSi to the bSi:POC ratio in both filtered and ST samples. All depths retain a significant overlap of the SSF and LSF bSi:POC, although median LSF values appear slightly higher in the deeper water column.

4. Discussion

4.1. The Size Distribution of POC, PIC, and bSi

From this global compilation of size-fractionated particulate data, we can probe the relative importance of certain organism groups to the overall budgets of POC, PIC, and bSi. Integrating the median binned concentrations plotted in Figure 6, we estimate the relative proportion of POC, PIC, and bSi found in the small and large filtered size fractions. The SSF makes up 77% of the POC pool in the upper 200 m, confirming the predominance of SSF POC in the upper ocean (Lam et al., 2018). This finding is consistent with independent estimates suggesting that the majority of surface ocean biomass is produced by small-sized phytoplankton and bacteria (Bar-On & Milo, 2019). Larger, less abundant material caught on the LSF has multiple sources: Larger organisms, aggregates of smaller particles and organisms, and/or fecal pellets. Because many large organisms are capable of swimming, they are likely to evade capture by pumps. Instead, most of the LSF is probably composed of dead and/or packaged material derived from smaller organisms.

The size distributions of PIC and bSi also reflect the biological production and subsequent processing of these phases. The SSF contains 76% of all PIC above 200 m, consistent with the high production of coccolith calcite relative to other calcifiers (Subhas et al., 2022; Ziveri et al., 2023). Pteropods, which are large aragonitic zooplankton, will primarily be collected in the LSF (Bednarsek et al., 2012; Dong et al., 2019). Calcitic planktic foraminifera will also be primarily collected in the LSF (Takahashi & Be, 1984). According to our estimates, the LSF contributes ∼24% to the upper ocean's PIC budget, leaving foraminifera and pteropods as minor contributors to global PIC inventories as determined by LVPs. However, we note that pteropods are swimming organisms and may not be captured effectively via filtration. Just under half of all bSi is found in the SSF. Diatoms span the LSF filter cutoff of 51 μm (Miklasz & Denny, 2010), and our analyses suggest that small and large diatoms produce roughly equal amounts of bSi.

Compared with the upper 200 m, whole-ocean inventories of both PIC and bSi are shifted further toward the SSF. For the entire water column the SSF accounts for 79%, 82%, and 50% of POC, PIC, and bSi, respectively. The shift in PIC toward smaller-sized particles may be either driven by the preferential dissolution of PIC associated with larger particles (Section 4.4), or by the shifting of PIC from the LSF to the SSF. This shift could be driven by the disaggregation of larger particle aggregates, or by the dissolution and fragmentation of larger pteropod shells and foraminiferal tests. Aggregation and disaggregation dynamics for bSi are harder to diagnose, due to the relatively constant ratio of SSF to LSF bSi in our data set (Figure 2c). We note that both GEOTRACES expeditions represented in this data set have sampled relatively quiescent, low-productivity regions of the Atlantic (GA03) and Pacific (GP16) basins. More sampling is clearly needed in productive, high-biomass regions and times of the year, such as the North Atlantic, North Pacific, and Southern Ocean basins.

4.2. Temporal and Spatial Patterns in Concentrations and Ratios

The spatial and temporal distributions of POC, PIC, and bSi appear to be related to distinct modes of phytoplankton production and export (Figures 2–4, Bach et al., 2016; Lam et al., 2011). For example, Station ALOHA shows almost identical PIC:POC across all particle types (Figure 3h), suggesting a high degree of exchange between size classes with minimal fractionation of PIC and POC during packaging and export. Interestingly, we note the alignment of ST PIC:POC with the SSF and LSF distributions at K2 in August (Figure 3m), a post-bloom time period with low PIC standing stocks and fluxes (Bishop & Wood, 2008; Lamborg et al., 2008). In the oligotrophic North Atlantic basin, BATS shows a strong enrichment of PIC:POC in deep sediment traps relative to filtered fractions (Figure 3n). The contrast between ALOHA and BATS may be related to contrasting styles of carbonate production and export at these two locations.

Higher productivity regions such as the Equatorial Pacific (Figures 3a–3g), K2 in July (Figure 3l), and OSP (Figures 3i–3k), all show enriched PIC in sediment traps relative to the SSF and LSF. This enrichment can have implications for the regional efficiency of the biological pump. Higher ST PIC fluxes should increase particle ballast, and thus increase settling speeds of particulate material (Laurenceau-Cornec et al., 2020). This PIC enrichment has two potential drivers. First, large, foraminifera tests or pteropod shells could enhance PIC without any effect on the ballasting of POC, although pteropods have a relatively low PIC:POC (Bednarsek et al., 2012; Schmidt et al., 2014, see Section 4.3). Second, an enrichment of PIC:POC may also indicate that POC is degraded during the creation of larger particles, implying the loss of POC in highly productive waters and a reduction in the vertical transfer of POC into the deep ocean.

Unlike PIC:POC, Station ALOHA and both occupations of K2 demonstrate enriched ST bSi:POC (Figures 4h, 4l, and 4m). These observations suggest that diatom-associated POC is being consumed, creating large silica-rich particles. Silica-producing animals such as radiolarians may also play a role in silica production and export (Bishop & Wood, 2008; Lamborg et al., 2008). However, many radiolarians exhibit lower bSi:POC than diatoms (Monferrer et al., 2020). Therefore, both radiolarians and diatoms require the preferential degradation of POC to explain our observed trends in bSi:POC. Interestingly, the SSF and ST bSi:POC directly overlap at OSP across all time intervals, suggesting a tight correspondence between small-sized silica producers and export down to 1,000 m (Figures 4i and 4j). At times these ratios greatly exceed the Si:C production ratio in diatoms, which ranges from 0.15 to 0.3 globally (Brzezinksi, 1985; Brzezinski et al., 2003), and could suggest intense processing of diatom- and radiolarian-produced POC throughout the upper water column, even in the small size fraction (Lam & Bishop, 2007). High bSi:POC ratios persist into the deep ocean (Figure 7f), and the resulting opal-rich particles provide a mechanism for the delivery of silica to deep North Pacific sediments (Hou et al., 2019).

These temporal and regional differences in PIC:POC and bSi:POC suggest that modes of production, and the structures of regional food webs, all play a role in setting the ballasting potential of particulate material in the upper ocean. However, we note that despite these regional patterns, sediment traps are clearly enriched in mineral phases relative to LVPs (Figures 6 and 7). This mineral enrichment may be due to inherent differences in the PIC:POC of carbonate producers; it may also be driven by community metabolism. With the exception of larger calcifiers such as pteropods and foraminifera, large particle formation is a product of metabolic activity by microbes and animals that consumes organic carbon. After such processing, particulate material captured by sediment traps is depleted in POC relative to the total particulate inventory measured by LVPs, implicating other modes of POC transport for moving organic carbon into the mesopelagic and deep ocean (Boyd et al., 2019).

4.3. Sinking Velocities of Biomineralizing Organisms

The differences in the size distribution of PIC and bSi (Figures 2 and 7) pushed us to reconsider the combined effects of size and excess density on particle sinking rates. Particles containing either bSi (ρ_s = 2,090) or PIC (ρ_s = 2,710 kg m^{-3}) will sink faster than particles made only of POC (ρ_s = 1,060 kg m^{-3}), but the size of the dominant producers of these minerals will also play a role in how fast this material sinks on its own, in the absence of aggregation or fecal pellet production. We compare measured sinking rates of diatoms (Miklasz & Denny, 2010) and foraminifera (Takahashi & Be, 1984) with computed coccolithophore and pteropod sinking velocities using Stokes' law (Stokes, 1851). To calculate excess density, we assumed that these organisms are composed of a mineral fraction (f_{min}) and an organic material fraction (f_{OC}, assuming $f_{\mathrm{min}} + f_{\mathrm{OC}} = 1$). We used the above PIC and POC densities and measured mineral:POC ratios to estimate biogenic particle density, ρ_s:

$$\rho_s = (1 - \phi)(f_{\mathrm{OC}} * \rho_{\mathrm{OC}} + \rho_{\mathrm{min}} * f_{\mathrm{min}}) + \phi\rho_{\mathrm{sw}}. \quad (1)$$

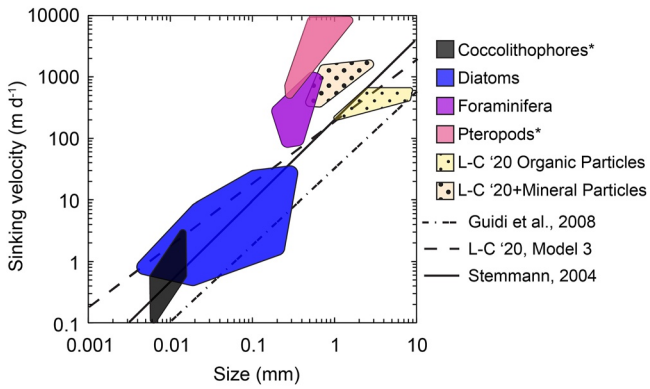

Figure 8. Particle size versus sinking velocity. The clouds of data represent sinking velocities of organism groups. Diatom and foraminifera sinking rates were taken from Miklasz and Denny (2010) and Takahashi and Be (1984), respectively. Coccolithophore and Pteropod sinking rates were calculates using Equations 1 and 2 in the text, using size and particulate inorganic carbon:particulate organic carbon data from Krumhardt et al. (2017) and Bednarsek et al. (2012), respectively. The data on organic-only and mineral-ballasted particles from Laurenceau-Cornec et al. (2020) (LC '20) are shown. Three semi-empirical models describing the sinking behavior of aggregates are also displayed.

Here, ρ_{OC} and ρ_{min} are the densities of organic carbon and mineral, respectively, and φ is the water content of the organism. We assumed that coccolithophores are 60% water ($\varphi = 0.6$, O'Brien et al., 2013), and that pteropods are 75% water (C. S. Davis & Wiebe, 1985). We used published ranges in PIC:POC ratios for coccolithophores (0.1–1.8, Krumhardt et al., 2017) and pteropods (0.27–0.73, Bednarsek et al., 2012) to calculate f_{min} Then, we used these excess densities to calculate a range in sinking velocities (U_s) for these organisms (Stokes, 1851):

$$U_s = \frac{g(\rho_s - \rho_{sw})D^2}{18\mu}, \tag{2}$$

where g is the gravitational acceleration in m s^{-2}, ρ_s is the density of the solid particle and ρ_{sw} is the density of seawater both in kg m^{-3}, D is the particle diameter in m, and μ is the fluid dynamic viscosity at 10°C (1.397×10^{-3} kg m^{-1} s^{-2}, Mostafa et al., 2010). Coccolithophore diameters ranged from 6 to 15 microns (Krumhardt et al., 2017); pteropod diameters ranged from 0.3 to 33 mm (Bednarsek et al., 2012). All organism sinking rates are shown in Figure 8 as polygons, drawn to capture the ranges in published and/or calculated organism sizes and sinking velocities.

Both foraminifera and pteropods produce large $CaCO_3$ structures, and are capable of sinking rapidly on their own (Figure 8, purple and pink clouds, respectively; Honjo et al., 2008; Takahashi & Be, 1984; Ziveri et al., 2023). These carbonate producers appear to sink as fast or faster than similarly sized organic aggregates that have been seeded with calcium carbonate (yellow clouds, Laurenceau-Cornec et al., 2020). Our calculations likely represent an upper bound to pteropod sinking velocities, because their large size translates to high particle Reynolds numbers and a breakdown of the relationship between the Stokes drag coefficient and Reynolds number (Dey et al., 2019). However, our computed pteropod sinking rates are largely consistent with reports of sinking rates >1 km day^{-1} (Byrne et al., 1984; Pasternak et al., 2017). Depending on their size and species, foraminifera sink between 100 and 1,000 m day^{-1}, within the range of published ST sinking velocities (Berelson, 2001). Such rapid sinking rates may help foraminifera and pteropod carcasses avoid any upper-ocean processing, and may help to explain their high abundances in deep sediment traps and surface sediments (Broecker & Clark, 2009; Boeuf et al., 2019; Chiu & Broecker, 2008; Dong et al., 2019; Subhas et al., 2019). Unlike pteropods, foraminifera have PIC:POC ratios of three or higher (C. V. Davis et al., 2017), and despite their overall low abundance (Ziveri et al., 2023), their presence in rapidly sinking ST material would help to explain the elevated PIC:POC in sediment traps relative to pumped samples in our data set (Figure 7c). Pteropods and coccolithophores exhibit similar PIC:POC (~0.1–2, Bednarsek et al., 2012; Krumhardt et al., 2017), both of which are higher than average surface LSF PIC:POC (Figure 6b), Thus the presence of pteropods would increase mean particle PIC:POC, but would not exert the same leverage as the presence of foraminifera.

Coccolithophores can exhibit very high PIC:POC but, because they are on the order of 10 μm in diameter, they sink very slowly (Figure 8, gray cloud, Bach et al., 2012; Honjo, 1976; Zhang et al., 2018). Diatoms produce a majority of the open-ocean silica, and while larger than coccolithophores, they often sink slower than 100 m d^{-1} on their own (Figure 8, blue cloud, Miklasz & Denny, 2010; Passow, 1991). Coccolithophores appear to produce a majority of pelagic PIC (Figure 2, Ziveri et al., 2023). However, their low inherent settling velocities means that they must aggregate to sink, necessitating biological processing and packaging (Bach et al., 2016; Bishop & Wood, 2008; Subhas et al., 2022).

The trophic processing of diatom and coccolithophore biomass clearly contributes ballast to fecal pellets and large marine aggregates found in sediment traps (Bach et al., 2016; Laurenceau-Cornec et al., 2015). In addition to the inherently lower density of bSi relative to PIC, the relative ballasting effectiveness of these two minerals will depend on their abundance relative to POC both in primary organisms and in marine aggregates (Takahashi, 1986). It will also depend on the lability of POC associated with diatom and coccolithophore biomass. For instance, several lines of evidence suggest that diatoms can be heavily stripped of their organic carbon, resulting in silica-rich, but POC-poor particles (Benitez-Nelson et al., 2007; Lam & Bishop, 2007). The fact that

Table 1
Surface (0–100 m) to 1,000 m (800–1,200 m) Ratios for Particulate Organic Carbon (POC) (Small Size Fraction, Large Size Fraction) or POC flux (Sediment Trap), Compared to 1,000 m:Surface Ratios in Particulate Inorganic Carbon:POC and Biogenic Silica:POC

0:1,000 m ratios in:	SSF	LSF	ST
POC or POC Flux (surf:1,000 m)	9	15	11
PIC:POC (1,000 m:surf)	5	2.5	2
bSi:POC (1,000 m:surf)	4	1.5	2

Note. In all cases, the increase in PIC:POC and bSi:POC is significantly less than the decrease in POC and POC flux.

the export of both coccolithophores and diatoms involves the digestion and remineralization of organic carbon raises the question of how resilient these mineral phases are to biologically mediated dissolution.

4.4. Shallow Dissolution and Recycling of Biogenic Minerals

Shallow remineralization of POC is a well-established feature of the global carbon cycle, and it reflects intense biological activity in the euphotic and mesopelagic zones of the global ocean (Martin et al., 1987; Pavia et al., 2019). Both SSF and LSF POC attenuate strongly from 0 to 1,000 m (Figure 2a), consistent with the active consumption and processing of organic carbon in the upper ocean. Shallow mineral dissolution is more controversial. The entire water column is undersaturated for bSi, and the dissolution of diatom frustules is thought to be accelerated by microbial respiration and enzyme activity (Bidle & Azam, 1999; Bidle et al., 2002). We observe a large attenuation of LVP bSi in the upper 1,000 m, consistent with a dissolution flux of bSi (Figure 2c). In contrast to silica saturation, the upper 1,000 m is typically supersaturated with respect to the dominant forms of $CaCO_3$, namely calcite and aragonite. Instead of being driven by ambient water column saturation, shallow PIC dissolution may be driven by metabolic processes that can locally decrease pH and saturation states (Milliman et al., 1999; Subhas et al., 2022). We also observe a decrease in the maximum PIC concentration with depth in both the large and small size fractions, suggesting a loss of PIC from the particulate pool (Figure 2b).

Dissolution is not the only process that can generate the observed attenuation profiles we observe. For all phases, aggregation-disaggregation dynamics will move material between SSF, LSF, and ST pools. If some portion of bSi and PIC forms larger aggregates and sinks, then the concentration profiles we measure will reflect a balance of biological production, consumption, aggregation, and sinking. Because we compare here all three particle types, we can test the hypothesis that mineral loss in the upper 1,000 m is balanced by mineral gain in the rapidly sinking ST pool. If the particle concentration profiles are solely controlled by particle removal via sinking, then decreases in LVP concentrations should be paired with increases in mineral flux in sediment traps. Alternatively, if dissolution is controlling the shape of these profiles, then we should see consistent decreases in LVP concentrations and ST fluxes.

These changes are easiest to diagnose relative to POC in a single size fraction. For instance, if SSF POC decreases by a factor of 10 between the surface and 1,000 m, and SSF PIC does not dissolve, then SSF PIC:POC should increase by a factor of 10. If PIC:POC increases by less than 10-fold, then SSF PIC must be dissolving along with POC, or PIC is being preferentially transferred to larger sedimenting particles. However, if the LSF and ST data also show a decoupling between POC attenuation and PIC:POC increase, then PIC dissolution must be occurring across all particle classes. We calculated the ratio of [POC] (or POC flux for sediment traps) between 0 and 1,000 m, and compared these values to the ratio of PIC:POC and bSi:POC between 0 and 1,000 m. Across all size classes, PIC:POC and bSi:POC increase less than predicted from the decrease in POC alone (Table 1).

The only process that can cause these consistent trends is the dissolution of bSi and PIC in the upper water column: Shifting mass between particle classes necessitates increases in these ratios in the larger particle classes. Interestingly, LSF and ST show a larger mismatch between POC attenuation and PIC:POC, bSi:POC increases than SSF (Table 1). We calculate a factor of 9 decrease in SSF POC, whereas PIC:POC and bSi:POC increase by factors of 5 and 4, respectively. In the LSF and ST pools, large decreases in POC from surface to 1,000 m well over a factor of 10 are paired with roughly a doubling of PIC:POC and bSi:POC, suggesting significant mineral loss coupled to the POC attenuation. The fact that the larger particle classes demonstrate more mineral dissolution suggests that microbial degradation in large aggregates, and zooplankton grazing and fecal pellet production, are actively contributing to the shallow dissolution of PIC and bSi (Bidle & Azam, 1999; Bidle et al., 2002; Bishop & Wood, 2008; Milliman et al., 1999; Subhas et al., 2022; Sulpis et al., 2021).

4.5. Fast-Sinking Particles and Practical Implications for Particle Sampling in the Ocean

The consistent trends we observe globally allow us to simplify the mineral:POC distributions in Figure 7 by plotting the median values in each depth range as a function of depth (Figure 9). Sediment trap material appears

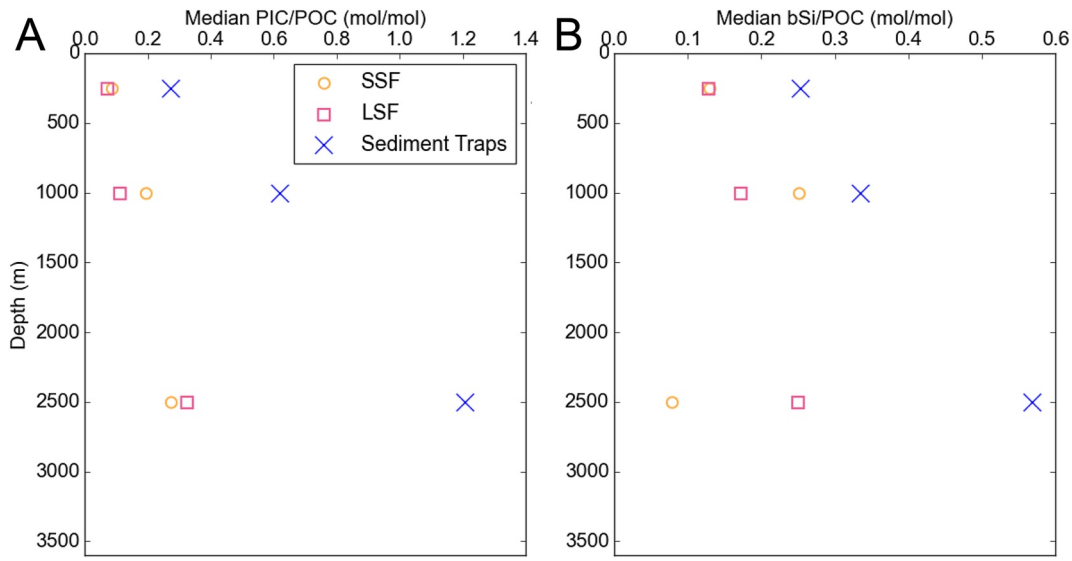

Figure 9. Median (a) particulate inorganic carbon:particulate organic carbon(POC) and (b) biogenic silica:POC in the 3 depth bins from Figure 7.

enriched in both PIC and bSi relative to filtered fractions at all depths. Enrichment of mineral ballast in export compared to standing stocks was previously shown in the Atlantic Ocean (Le Moigne et al., 2012); here we have extended this observation to the global ocean, and to all depths. The median SSF and LSF PIC:POC values are very similar to one another, suggesting that these pools are in constant exchange throughout the water column (Figure 9a). The median ST PIC:POC demonstrates a stronger increases with depth compared with the SSF and LSF. Below 1,500 m, we calculate a median PIC:POC of 1.2, meaning that more inorganic carbon is being delivered to the sediments than organic carbon. Similarly, the ST bSi:POC increases with depth, and below 1,500 m it is well above the mean Si:C production ratio of diatoms and other silica producers (Figure 7b, Brzezinski, 1985). In constrast, the SSF bSi:POC appears to be relatively constant with depth. Small particles will have higher surface area:volume, allowing greater contact with silica-undersaturated seawater per unit mass of silica.

Interestingly, both PIC:POC and bSi:POC continue to increase below the twilight zone suggesting continued modification of this rapidly sinking material, and this enrichment is strongest in ST material. It is possible that large aggregates continue respire POC to a greater extent than smaller particles. It is also possible that disaggregation of larger particles preferentially moves POC into the smaller size classes where it is subsequently respired (Amaral et al., 2022; Lam & Marchal, 2015). The practical result of this mineral enrichment is an increase in ballast and thus an increase in settling velocity of the large particles captured by sediment traps (Berelson, 2001). Assuming a 1 mm particle and 99% porosity, the increase in PIC:POC translates to an increase in settling velocity from 150 to 400 m day^{-1}. The increase in bSi:POC translates to an increase in settling velocity from 110 to 175 m day^{-1}, highlighting the reduced potential of bSi to ballast these larger particles.

Sediment traps have been used for decades in oceanographic studies, and can be deployed across a range of timescales from days to years (Berelson, 2001; Honjo, 1976; Honjo et al., 2008; Martin et al., 1987; Mouw et al., 2016; Wiebe et al., 1976). However, one repeated criticism of these tools is that they appear to miss smaller, slower-sinking particles that may contribute substantially to the biological carbon pump (Boyd et al., 2019; Henson et al., 2011). More recently, dedicated surveys of particle fields through programs like GEOTRACES have been amassing high-quality particle concentration data via LVPs (Lam et al., 2018). LVPs are typically deployed for hours at a time, and may miss the actively swimming component of biomass such as pteropods. The practical result of these methodologies is that they appear to sample very different portions of the particulate pool, particularly with respect to biogenic minerals (Figures 7 and 9). The majority of particle mass appears to be POC-rich, whereas sinking particles appear to be enriched in mineral phases (Figure 9). These limitations place constraints on the ability for any one methodology to provide a complete picture of particle cycling in the ocean, especially considering that these methods are measuring different quantities (concentration and flux). For example, LVP-based measurements of uranium-series disequilibrium may sufficiently capture POC fluxes,

but will miss a mineral-rich, fast-sinking component of the total mass flux (Bacon & Anderson, 1982; Henson et al., 2011; Pavia et al., 2019). Conversely, sediment traps likely miss key processes involved in the cycling of organic carbon, because a majority of this phase is associated with small particles with long ocean residence times and slow sinking rates (Boyd et al., 2019). We suggest that more expeditions consider pairing LVP deployments with sediment traps, in order to capture a fuller picture of marine particle dynamics.

5. Conclusions

The marine biological carbon pump functions in part because of the ballasting effect of dense mineral phases like calcium carbonate and opal. Here, we have demonstrated that the distributions and fluxes of POC, PIC, and bSi are linked not only to the ecology of their production, but are influenced by the subsequent processing of this material. Using all available data, more than 75% of POC and PIC, and roughly half of bSi, is found in particles smaller than 51 microns. We conclude that coccolithophores and diatoms produce a majority of the PIC and bSi at the ocean surface, but are too small to sink rapidly, necessitating the packaging of this primary material into larger aggregates. In contrast, larger calcifying organisms such as foraminifera and pteropods are heavily ballasted enough to sink rapidly on their own, contributing to the overall PIC flux but likely not contributing to the ballasting of exogenous POC. The material captured by sediment traps appears to be elevated in PIC and bSi relative to filtered samples, suggesting a preferential fractionation of mineral phases into large, rapidly sinking aggregates. This fractionation is driven by the trophic interactions that create aggregates in the first place, which provides a mechanism for the metabolic dissolution of mineral phases in the euphotic and mesopelagic zones. Furthermore, this fractionation means that a majority of the mineral flux to the seafloor is likely accomplished through large, heavily ballasted particles, rather than through smaller particles more enriched in POC. We caution that LVP-based sampling techniques likely miss a portion of this heavily ballasted particle field.

Data Availability Statement

Compiled LVP data can be accessed through BCO-DMO (Pavia et al., 2022, https://doi.org/10.26008/1912/bco-dmo.883965.1), which includes the data of Bishop and Lam (2022, https://doi.org/10.26008/1912/bco-dmo.884057.1). The compiled sediment trap data can be accessed through Mouw et al. (2016).

Acknowledgments
A.V.S. Acknowledges funding from the National Science Foundation (NSF-GCR 2020878 and NSF-OCE 1923998). F.J.P. acknowledges support from the Stanback Postdoctoral Scholarship. GEOTRACES LVP data were produced from NSF-OCE 0963026 and 1518110 to P.J.L. We acknowledge the helpful and constructive comments from two anonymous reviewers and the Associate Editor. We acknowledge that the Woods Hole Oceanographic Institution is located on, and benefits directly from, the stolen lands of the Mashpee Wampanoag tribe.

References

Alldredge, A. L., & Gotschalk, C. (1988). In situ settling behavior of marine snow. *Limnology & Oceanography*, *33*(3), 339–351. https://doi.org/10.4319/lo.1988.33.3.0339

Amaral, V. J., Lam, P. J., Marchal, O., Roca-Marti, M., Fox, J., & Nelson, N. B. (2022). Particle cycling rates at Station P as estimated from the inversion of POC concentration data. *Elementa: Science of the Anthropocene*, *10*(1), 00018. https://doi.org/10.1525/elementa.2021.00018

Bach, L. T., Boxhammer, T., Larsen, A., Hildebrandt, N., Schulz, K. G., & Riebesell, U. (2016). Influence of plankton community structure on the sinking velocity of marine aggregates. *Global Biogeochemical Cycles*, *30*(8), 1145–1165. https://doi.org/10.1002/2016gb005372

Bach, L. T., Riebesell, U., Sett, S., Febiri, S., Rzepka, P., & Schulz, K. G. (2012). An approach for particle sinking velocity measurements in the 3–400 μm size range and considerations on the effect of temperature on sinking rates. *Marine Biology*, *159*(8), 1853–1864. https://doi.org/10.1007/s00227-012-1945-2

Bacon, M. P., & Anderson, R. F. (1982). Distribution of thorium isotopes between dissolved and particulate forms in the deep sea. *Journal of Geophysical Research*, *87*(C3), 2045–2056. https://doi.org/10.1029/jc087ic03p02045

Baker, C. A., Estapa, M. L., Iversen, M., Lampitt, R., & Buesseler, K. (2020). Are all sediment traps created equal? An intercomparison study of carbon export methodologies at the PAP-SO site. *Progress in Oceanography*, *184*, 102317. https://doi.org/10.1016/j.pocean.2020.102317

Bar-On, Y. M., & Milo, R. (2019). The biomass composition of the oceans: A blueprint of our blue planet. *Cell*, *179*(7), 1451–1454. https://doi.org/10.1016/j.cell.2019.11.018

Bednaršek, N., Možina, J., Vogt, M., O'Brien, C., & Tarling, G. A. (2012). The global distribution of pteropods and their contribution to carbonate and carbon biomass in the modern ocean. *Earth System Science Data*, *4*(1), 167–186. https://doi.org/10.5194/essd-4-167-2012

Benitez-Nelson, C. R., Bidigare, R. R., Dickey, T. D., Landry, M. R., Leonard, C. L., Brown, S. L., et al. (2007). Mesoscale eddies drive increased silica export in the subtropical Pacific Ocean. *Science*, *316*(5827), 1017–1021. https://doi.org/10.1126/science.1136221

Berelson, W. M. (2001). Particle settling rates increase with depth in the ocean. *Deep-Sea Research Part II*, *49*(1–3), 237–251. https://doi.org/10.1016/s0967-0645(01)00102-3

Bidle, K. D., & Azam, F. (1999). Accelerated dissolution of diatom silica by marine bacterial assemblages. *Nature*, *397*(6719), 508–512. https://doi.org/10.1038/17351

Bidle, K. D., Manganelli, M., & Azam, F. (2002). Regulation of oceanic silicon and carbon preservation by temperature control on bacteria. *Science*, *298*(5600), 1980–1984. https://doi.org/10.1126/science.1076076

Bishop, J. K. B., & Lam, P. J. (2022). Compilation of MULVFS size-fractionated POC, PIC, and bSi data from 17 cruises conducted between 1973 and 2005. Biological and chemical Oceanography data management office (BCO-DMO). (Version 1) Version Date 2022-11-21. https://doi.org/10.26008/1912/bco-dmo.884057.1

Bishop, J. K. B., Collier, R. W., Kettens, D. R., & Edmond, J. M. (1980). The chemistry, biology, and vertical flux of particulate matter from the upper 1500 m of the Panama Basin. *Deep-Sea Research*, *27*(8), 615–640. https://doi.org/10.1016/0198-0149(80)90077-1

Bishop, J. K. B., Edmond, J. M., Ketten, D. R., Bacon, M. P., & Silker, W. B. (1977). Chemistry, biology, and vertical flux of particulate matter from upper 400 M of equatorial Atlantic Ocean. *Deep-Sea Research*, *24*(6), 511–548. https://doi.org/10.1016/0146-6291(77)90526-4

Bishop, J. K. B., Schupack, D., Sherrell, R. M., & Conte, M. (1985). Mapping strategies in chemical oceanography. *Advances in Chemistry*, 155–175. https://doi.org/10.1021/ba-1985-0209.ch009

Bishop, J. K. B., & Wood, T. J. (2008). Particulate matter chemistry and dynamics in the twilight zone at VERTIGO ALOHA and K2 sites. *Deep Sea Research Part I: Oceanographic Research Papers*, *55*(12), 1684–1706. https://doi.org/10.1016/j.dsr.2008.07.012

Boeuf, D., Edwards, B. R., Eppley, J. M., Hu, S. K., Poff, K. E., Romano, A. E., et al. (2019). Biological composition and microbial dynamics of sinking particulate organic matter at abyssal depths in the oligotrophic open ocean. *Proceedings of the National Academy of Sciences of the United States of America*, *116*(24), 11824–11832. https://doi.org/10.1073/pnas.1903080116

Boyd, P. W., Claustre, H., Levy, M., Siegel, D. A., & Weber, T. (2019). Multi-faceted particle pumps drive carbon sequestration in the ocean. *Nature*, *568*(7752), 1–9. https://doi.org/10.1038/s41586-019-1098-2

Broecker, W., & Clark, E. (2009). Ratio of coccolith $CaCO_3$ to foraminifera $CaCO_3$ in late Holocene deep sea sediments. *Paleoceanography*, *24*(3), 1–11. https://doi.org/10.1029/2009pa001731

Brzezinski, M. A. (1985). The Si:C:N ratio of marine diatoms: Interspecific variability and the effect of some environmental variables. *Journal of Phycology*, *21*(3), 347–357. https://doi.org/10.1111/j.0022-3646.1985.00347.x

Brzezinski, M. A., Dickson, M.-L., Nelson, D. M., & Sambrotto, R. (2003). Ratios of Si, C and N uptake by microplankton in the Southern Ocean. *Deep Sea Research Part II: Topical Studies in Oceanography*, *50*(3–4), 619–633. https://doi.org/10.1016/s0967-0645(02)00587-8

Buesseler, K. O., Ball, L., Andrews, J., Cochran, J. K., Hirschberg, D. J., Bacon, M. P., et al. (2001). Upper ocean export of particulate organic carbon and biogenic silica in the Southern Ocean along 170°W. *Deep Sea Research Part II: Topical Studies in Oceanography*, *48*(19–20), 4275–4297. https://doi.org/10.1016/s0967-0645(01)00089-3

Buesseler, K. O., Trull, T. W., Steinberg, D. K., Silver, M. W., Siegel, D. A., Saitoh, S.-I., et al. (2008). VERTIGO (VERtical transport in the global ocean): A study of particle sources and flux attenuation in the North Pacific. *Deep Sea Research Part II: Topical Studies in Oceanography*, *55*(14–15), 1522–1539. https://doi.org/10.1016/j.dsr2.2008.04.024

Byrne, R. H., Acker, J. G., Betzer, P. R., Feely, R. A., & Cates, M. H. (1984). Water column dissolution of aragonite in the Pacific Ocean. *Nature*, *312*(5992), 321–326. https://doi.org/10.1038/312321a0

Cael, B. B., Bisson, K., Conte, M., Duret, M. T., Follett, C. L., Henson, S. A., et al. (2021). Open ocean particle flux variability from surface to seafloor. Geophysical Research Letters, 48(9), e2021GL092895. Portico. https://doi.org/10.1029/2021gl092895

Chiu, T., & Broecker, W. S. (2008). Toward better paleocarbonate ion reconstructions: New insights regarding the $CaCO_3$ size index. *Paleoceanography*, *23*(2), PA2216. https://doi.org/10.1029/2008pa001599

Conte, M. H. (2022). Mass flux and concentrations of bulk components (carbonate, organic carbon/nitrogen, lithogenics, opal) and elements in the flux at 500m, 1500m and 3200m depths from the OFP sediment trap time-series in the northern Sargasso Sea. *Biological and Chemical Oceanography Data Management Office (BCO-DMO)*. https://doi.org/10.26008/1912/bco-dmo.784396.1

Davis, C. S., & Wiebe, P. H. (1985). Macrozooplankton biomass in a warm-core Gulf Stream ring: Time series changes in size structure, taxonomic composition, and vertical distribution. *Journal of Geophysical Research*, *90*(C5), 8871–8884. https://doi.org/10.1029/jc090ic05p08871

Davis, C. V., Rivest, E. B., Hill, T. M., Gaylord, B., Russell, A. D., & Sanford, E. (2017). Ocean acidification compromises a planktic calcifier with implications for global carbon cycling. *Scientific Reports*, *7*(1), 2225. https://doi.org/10.1038/s41598-017-01530-9

Dey, S., Ali, S. Z., & Padhi, E. (2019). Terminal fall velocity: The legacy of Stokes from the perspective of fluvial hydraulics. *Proceedings of the Royal Society A: Mathematical, Physical & Engineering Sciences*, *475*(2228), 20190277. https://doi.org/10.1098/rspa.2019.0277

Dong, S., Berelson, W. M., Rollins, N. E., Subhas, A. V., Naviaux, J. D., Celestian, A. J., et al. (2019). Aragonite dissolution kinetics and calcite/aragonite ratios in sinking and suspended particles in the North Pacific. *Earth and Planetary Science Letters*, *515*, 1–12. https://doi.org/10.1016/j.epsl.2019.03.016

Dong, S., Wang, X. T., Subhas, A. V., Pavia, F. J., Adkins, J. F., & Berelson, W. M. (2022). Depth profiles of suspended carbon and nitrogen along a North Pacific transect: Concentrations, isotopes, and ratios. *Limnology & Oceanography*, *67*(1), 247–260. https://doi.org/10.1002/lno.11989

Dunne, J. P., Sarmiento, J. L., & Gnanadesikan, A. (2007). A synthesis of global particle export from the surface ocean and cycling through the ocean interior and on the seafloor. *Global Biogeochemical Cycles*, *21*(4), GB4006. https://doi.org/10.1029/2006gb002907

Feely, R. A., Sabine, C. L., Lee, K., Millero, F. J., Lamb, M. F., Greeley, D., et al. (2002). In situ calcium carbonate dissolution in the Pacific Ocean. *Global Biogeochemical Cycles*, *16*(4), 91-1–91-12. https://doi.org/10.1029/2002gb001866

Fowler, S. W., & Knauer, G. A. (1986). Role of large particles in the transport of elements and organic compounds through the oceanic water column. *Progress in Oceanography*, *16*(3), 147–194. https://doi.org/10.1016/0079-6611(86)90032-7

Frankignoulle, M., Canon, C., & Gattuso, J. (1994). Marine calcification as a source of carbon dioxide: Positive feedback of increasing atmospheric CO_2. *Limnology & Oceanography*, *39*(2), 458–462. https://doi.org/10.4319/lo.1994.39.2.0458

Guidi, L., Jackson, G. A., Stemmann, L., Miquel, J. C., Picheral, M., & Gorsky, G. (2008). Relationship between particle size distribution and flux in the mesopelagic zone. *Deep Sea Research Part I: Oceanographic Research Papers*, *55*(10), 1364–1374. https://doi.org/10.1016/jdsr.2008.05.014

Henson, S. A., Sanders, R., Madsen, E., Morris, P. J., Moigne, F. L., & Quartly, G. D. (2011). A reduced estimate of the strength of the ocean's biological carbon pump. *Geophysical Research Letters*, *38*(4), L04606. https://doi.org/10.1029/2011gl046735

Honjo, S. (1976). Coccoliths: Production, transportation and sedimentation. *Marine Micropaleontology*, *1*, 65–79. https://doi.org/10.1016/0377-8398(76)90005-0

Honjo, S., Dymond, J., Collier, R., & Manganini, S. J. (1995). Export production of particles to the interior of the equatorial Pacific Ocean during the 1992 EqPac experiment. *Deep Sea Research Part II: Topical Studies in Oceanography*, *42*(2–3), 831–870. https://doi.org/10.1016/0967-0645(95)00034-n

Honjo, S., Manganini, S. J., Krishfield, R. A., & Francois, R. (2008). Particulate organic carbon fluxes to the ocean interior and factors controlling the biological pump: A synthesis of global sediment trap programs since 1983. *Progress in Oceanography*, *76*(3), 217–285. https://doi.org/10.1016/j.pocean.2007.11.003

Hou, Y., Hammond, D. E., Berelson, W. M., Kemnitz, N., Adkins, J. F., & Lunstrum, A. (2019). Spatial patterns of benthic silica flux in the North Pacific reflect upper ocean production. *Deep Sea Research Part I: Oceanographic Research Papers*, *148*, 25–33. https://doi.org/10.1016/j.dsr.2019.04.013

Humphreys, M. P., Daniels, C. J., Wolf-Gladrow, D. A., Tyrrell, T., & Achterberg, E. P. (2018). On the influence of marine biogeochemical processes over CO_2 exchange between the atmosphere and ocean. *Marine Chemistry*, *199*, 1–11. https://doi.org/10.1016/j.marchem.2017.12.006

Klaas, C., & Archer, D. E. (2002). Association of sinking organic matter with various types of mineral ballast in the deep sea: Implications for the rain ratio. *Global Biogeochemical Cycles*, *16*(4), 63-1–63-14. https://doi.org/10.1029/2001gb001765

Krumhardt, K. M., Lovenduski, N. S., Iglesias-Rodriguez, M. D., & Kleypas, J. A. (2017). Coccolithophore growth and calcification in a changing ocean. *Progress in Oceanography*, *159*, 276–295. https://doi.org/10.1016/j.pocean.2017.10.007

Lam, P. J., & Bishop, J. K. B. (2007). High biomass, low export regimes in the Southern Ocean. *Deep Sea Research Part II: Topical Studies in Oceanography*, *54*(5–7), 601–638. https://doi.org/10.1016/j.dsr2.2007.01.013

Lam, P. J., Doney, S. C., & Bishop, J. K. B. (2011). The dynamic ocean biological pump: Insights from a global compilation of particulate organic carbon, $CaCO_3$, and opal concentration profiles from the mesopelagic. *Global Biogeochemical Cycles*, *25*(3), GB3009. https://doi.org/10.1029/2010gb003868

Lam, P. J., Lee, J.-M., Heller, M. I., Mehic, S., Xiang, Y., & Bates, N. R. (2018). Size-fractionated distributions of suspended particle concentration and major phase composition from the U.S. GEOTRACES Eastern Pacific Zonal Transect (GP16). *Marine Chemistry*, *201*, 90–107. https://doi.org/10.1016/j.marchem.2017.08.013

Lam, P. J., & Marchal, O. (2015). Insights into particle cycling from thorium and particle data. *Annual Review of Marine Science*, *7*(1), 159–184. https://doi.org/10.1146/annurev-marine-010814-015623

Lam, P. J., Ohnemus, D. C., & Auro, M. E. (2015). Size-fractionated major particle composition and concentrations from the US GEOTRACES North Atlantic zonal transect. *Deep Sea Research Part II: Topical Studies in Oceanography*, *116*, 303–320. https://doi.org/10.1016/j.dsr2.2014.11.020

Lamborg, C. H., Buesseler, K. O., & Lam, P. J. (2008). Sinking fluxes of minor and trace elements in the North Pacific Ocean measured during the VERTIGO program. *Deep Sea Research Part II: Topical Studies in Oceanography*, *55*(14–15), 1564–1577. https://doi.org/10.1016/j.dsr2.2008.04.012

Laurenceau-Cornec, E. C., Moigne, F. A. C. L., Gallinari, M., Moriceau, B., Toullec, J., Iversen, M. H., et al. (2020). New guidelines for the application of Stokes' models to the sinking velocity of marine aggregates. *Limnology & Oceanography*, *65*(6), 1264–1285. https://doi.org/10.1002/lno.11388

Laurenceau-Cornec, E. C., Trull, T. W., Davies, D. M., Bray, S. G., Doran, J., Planchon, F., et al. (2015). The relative importance of phytoplankton aggregates and zooplankton fecal pellets to carbon export: Insights from free-drifting sediment trap deployments in naturally iron-fertilised waters near the Kerguelen Plateau. *Biogeosciences*, *12*(4), 1007–1027. https://doi.org/10.5194/bg-12-1007-2015

Le Moigne, F. A. C., Sanders, R. J., Villa-Alfageme, M., Martin, A. P., Pabortsava, K., Planquette, H., et al. (2012). On the proportion of ballast versus non-ballast associated carbon export in the surface ocean. *Geophysical Research Letters*, *39*(15), L15610. https://doi.org/10.1029/2012gl052980

Martin, J. H., Knauer, G. A., Karl, D. M., & Broenkow, W. W. (1987). VERTEX: Carbon cycling in the northeast Pacific. *Deep-Sea Research*, *34*(2), 267–285. https://doi.org/10.1016/0198-0149(87)90086-0

McCave, I. N. (1975). Vertical flux of particles in the ocean. *Deep-Sea Research and Oceanographic Abstracts*, *22*(7), 491–502. https://doi.org/10.1016/0011-7471(75)90022-4

McCave, I. N. (1984). Size spectra and aggregation of suspended particles in the deep ocean. *Deep-Sea Research, Part A: Oceanographic Research Papers*, *31*(4), 329–352. https://doi.org/10.1016/0198-0149(84)90088-8

Miklasz, K. A., & Denny, M. W. (2010). Diatom sinkings speeds: Improved predictions and insight from a modified Stokes' law. *Limnology & Oceanography*, *55*(6), 2513–2525. https://doi.org/10.4319/lo.2010.55.6.2513

Milliman, J. D., Troy, P. J., Balch, W. M., Adams, A. K., Li, Y. H., & Mackenzie, F. (1999). Biologically mediated dissolution of calcium carbonate above the chemical lysocline? *Deep-Sea Research*, *46*(10), 1653–1669. https://doi.org/10.1016/s0967-0637(99)00034-5

Monferrer, N. L., Boltovskoy, D., Tréguer, P., Sandin, M. M., Not, F., & Leynaert, A. (2020). Estimating biogenic silica production of Rhizaria in the global ocean. *Global Biogeochemical Cycles*, *34*(3), e2019GB006286. https://doi.org/10.1029/2019gb006286

Mostafa, H. S., John, H. L. V., & Zubair, S. M. (2010). Thermophysical properties of seawater: A review of existing correlations and data. *Desalination and Water Treatment*, *16*(1–3), 354–380. https://doi.org/10.5004/dwt.2010.1079

Mouw, C. B., Barnett, A., McKinley, G. A., Gloege, L., & Pilcher, D. (2016). Global ocean particulate organic carbon flux merged with satellite parameters. *Earth System Science Data*, *8*(2), 531–541. https://doi.org/10.5194/essd-8-531-2016

O'Brien, C. J., Peloquin, J. A., Vogt, M., Heinle, M., Gruber, N., Ajani, P., et al. (2013). Global marine plankton functional type biomass distributions: Coccolithophores. *Earth System Science Data*, *5*(2), 259–276. https://doi.org/10.5194/essd-5-259-2013

Passow, U. (1991). Species-specific sedimentation and sinking velocities of diatoms. *Marine Biology*, *108*(3), 449–455. https://doi.org/10.1007/bf01313655

Passow, U., & De La Rocha, C. L. (2006). Accumulation of mineral ballast on organic aggregates: Mineral ballast and organic aggregates. *Global Biogeochemical Cycles*, *20*(1), GB1013. https://doi.org/10.1029/2005gb002579

Pasternak, A. F., Drits, A. V., & Flint, M. V. (2017). Feeding, egg production, and respiration rate of pteropods *Limacina* in Arctic seas. *Oceanology*, *57*(1), 122–129. https://doi.org/10.1134/s000143701701012x

Pavia, F. J., Anderson, R. F., Lam, P. J., Cael, B. B., Vivancos, S. M., Fleisher, M. Q., et al. (2019). Shallow particulate organic carbon regeneration in the South Pacific Ocean. *Proceedings of the National Academy of Sciences of the United States of America*, *116*(20), 9753–9758. https://doi.org/10.1073/pnas.1901863116

Pavia, F. J., Dong, S., Lam, P. J., & Subhas, A. V. (2022). Compiled global dataset of PIC/POC and bSi concentrations measured by in situ pumps on multiple research cruises conducted from between 1973 and 2013. Biological and Chemical Oceanography Data Management Office (BCO-DMO). (Version 1) Version Date 2022-11-18. https://doi.org/10.26008/1912/bco-dmo.883965.1

Sarmiento, J. L., Dunne, J., Gnanadesikan, A., Key, R. M., Matsumoto, K., & Slater, R. (2002). A new estimate of the $CaCO_3$ to organic carbon export ratio. *Global Biogeochemical Cycles*, *16*(4), 54-1–54-12. https://doi.org/10.1029/2002gb001919

Schmidt, K., De La Rocha, C. L., Gallinari, M., & Cortese, G. (2014). Not all calcite ballast is created equal: Differing effects of foraminiferan and coccolith calcite on the formation and sinking of aggregates. *Biogeosciences*, *11*(1), 135–145. https://doi.org/10.5194/bg-11-135-2014

Stokes, G. G. (1851). *On the effect of the internal friction offluids on the motion of pendulums*. Transactions of the Cambridge Philosophical Society, (Vol. 9, pp. 8–106).

Subhas, A. V., Dong, S., Naviaux, J. D., Rollins, N. E., Ziveri, P., Gray, W., et al. (2022). Shallow calcium carbonate cycling in the North Pacific Ocean. *Global Biogeochemical Cycles*, *36*(5), e2022GB007388. https://doi.org/10.1029/2022gb007388

Subhas, A. V., McCorkle, D. C., Quizon, A., McNichol, A. P., & Long, M. H. (2019). Selective preservation of coccolith calcite in Ontong-Java Plateau sediments. *Paleoceanography and Paleoclimatology*, *34*(12), 2141–2157. https://doi.org/10.1029/2019pa003731

Sulpis, O., Jeansson, E., Dinauer, A., Lauvset, S. K., & Middelburg, J. J. (2021). Calcium carbonate dissolution patterns in the ocean. *Nature Geoscience*, *14*, 1–6. https://doi.org/10.1038/s41561-021-00743-y

Takahashi, K. (1986). Seasonal fluxes of pelagic diatoms in the subarctic Pacific, 1982–1983. *Deep-Sea Research, Part A: Oceanographic Research Papers*, *33*(9), 1225–1251. https://doi.org/10.1016/0198-0149(86)90022-1

Takahashi, K., & Be, A. W. H. (1984). Planktonic foraminifera: Factors controlling sinking speeds. *Deep-Sea Research, Part A: Oceanographic Research Papers*, *31*(12), 1477–1500. https://doi.org/10.1016/0198-0149(84)90083-9

Timothy, D. A., Wong, C. S., Barwell-Clarke, J. E., Page, J. S., White, L. A., & Macdonald, R. W. (2013). Climatology of sediment flux and composition in the subarctic Northeast Pacific Ocean with biogeochemical implications. *Progress in Oceanography*, *116*, 95–129. https://doi.org/10.1016/j.pocean.2013.06.017

Volk, T., & Hoffert, M. I. (1985). The carbon cycle and atmospheric CO_2: Natural variations Archean to present. *Geophysical Monograph Series*, 99–110. https://doi.org/10.1029/gm032p0099

Wiebe, P. H., Boyd, S. H., & Winget, C. (1976). Particulate matter sinking to the deep-sea floor at 2000 m in the Tongue of the Ocean, Bahamas with a description of a new sedimentation trap. *Journal of Marine Research*, *34*, 341–354l.

Wong, C. S., Whitney, F. A., Crawford, D. W., Iseki, K., Matear, R. J., Johnson, W. K., et al. (1999). Seasonal and interannual variability in particle fluxes of carbon, nitrogen and silicon from time series of sediment traps at Ocean Station P, 1982–1993: Relationship to changes in subarctic primary productivity. *Deep Sea Research Part II: Topical Studies in Oceanography*, *46*(11–12), 2735–2760. https://doi.org/10.1016/s0967-0645(99)00082-x

Xiang, Y., Lam, P. J., Burd, A. B., & Hayes, C. T. (2022). Estimating mass flux from size-fractionated filtered particles: Insights into controls on sinking velocities and mass fluxes in recent U.S. GEOTRACES cruises. *Global Biogeochemical Cycles*, *36*(4), e2021GB007292. https://doi.org/10.1029/2021gb007292

Zhang, H., Stoll, H., Bolton, C., Jin, X., & Liu, C. (2018). Technical note: A refinement of coccolith separation methods: Measuring the sinking characteristics of coccoliths. *Biogeosciences*, *15*(15), 4759–4775. https://doi.org/10.5194/bg-15-4759-2018

Ziveri, P., Gray, W. R., Ortiz, G. A. I., Manno, C., Grelaud, M., Incarbona, A., et al. (2023). Pelagic carbonate production in the North Pacific Ocean. In *Press at nature communications*.